

Journal of Materials Chemistry A

Accepted Manuscript



This is an *Accepted Manuscript*, which has been through the Royal Society of Chemistry peer review process and has been accepted for publication.

Accepted Manuscripts are published online shortly after acceptance, before technical editing, formatting and proof reading. Using this free service, authors can make their results available to the community, in citable form, before we publish the edited article. We will replace this *Accepted Manuscript* with the edited and formatted *Advance Article* as soon as it is available.

You can find more information about *Accepted Manuscripts* in the [Information for Authors](#).

Please note that technical editing may introduce minor changes to the text and/or graphics, which may alter content. The journal's standard [Terms & Conditions](#) and the [Ethical guidelines](#) still apply. In no event shall the Royal Society of Chemistry be held responsible for any errors or omissions in this *Accepted Manuscript* or any consequences arising from the use of any information it contains.

Facile fabrication of α -FeOOH nanorod/RGO composite: A robust photocatalyst for reduction of Cr(VI) under visible light irradiation

Deepak Kumar Padhi and Kulamani Parida*

Colloids and Materials Chemistry Department, CSIR-Institute of Minerals and Materials Technology, Bhubaneswar – 751 013, Odisha, INDIA

* Corresponding author

E-mail: paridakulamani@yahoo.com

Tel. No. +91-674-2379425

Fax. +91-674-2581637

Abstract

A facile one step hydrothermal route has been adopted for the in-situ deposition of α -FeOOH nanorods over reduced graphene oxide sheets (RGO) where sodium hydroxide plays a dual role for the growth of α -FeOOH nanorods and reduction of graphene oxide (GO) to RGO. The crystallographic, microscopic, and spectroscopic properties of the as-synthesized α -FeOOH nanorod/RGO composites were explored by XRD, Raman, DRUV-vis, PL, TRPL, XPS, FESEM, TEM and photoelectrochemical measurement. The α -FeOOH nanorod/RGO composite displays superior photocatalytic activity towards the reduction of hexavalent chromium [Cr(VI)] compared to neat α -FeOOH nanorod under visible light irradiation. The extended Π -conjugated flat 2D layer of graphene plays a crucial role in enhancing the photocatalytic activity of α -FeOOH nanorod by channelizing the photoexcited electrons on its surface. This leads to minimise the electron-hole recombination which is successfully derived from photoluminescence study, time-resolved photoluminescence spectra and photoelectrochemical measurement of α -FeOOH nanorod/RGO composites. The time resolved decay measurements showed longer average decay time ($\langle\tau\rangle$) for 3wt% RGO loaded α -FeOOH of the order of 4.13 ns than that of the neat α -FeOOH (2.536 ns). The improved photocurrent generation (nearly 3 times higher than the neat α -FeOOH nanorod) and low photoluminescence (PL) intensity of α -FeOOH nanorod/RGO composite is due to the well decoration and strong attachment of α -FeOOH nanorods over RGO sheets which significantly enhances its photocatalytic activity.

KEYWORDS: *α -FeOOH nanorod/RGO composite, Hydrothermal reaction, Electron transfer, Photocurrent, Hexavalent chromium reduction.*

1. Introduction

Hexavalent chromium [Cr(VI)] and trivalent chromium [Cr(III)] are the most common forms of chromium. These two forms of Cr play different role in accordance to their oxidation state.^[1] The Cr species having +3 oxidation state plays a vital role in the plant and animal metabolism. But +6 oxidation state species is highly toxic to plant as well as animals and is a major contaminant in wastewaters arising from different industry.^[2,3] Now a days photocatalytic reduction of Cr(VI) by semiconductor photocatalyst is one of the emerging technique for removal of Cr(VI) contamination.^[4] In this regards, many people have developed several materials for the photocatalytic reduction of Cr(VI) under ultraviolet and visible light irradiation.^[5-8] But the flash recombination of electron-hole is the major drawback of a semiconductor photocatalyst which reduces its photocatalytic efficiency.

On the other hand, Graphene is one of the emerging material, possesses a lot of potential to minimise the recombination of electron-hole of a semiconductor during photochemical reaction. It consists of flat 2D-Sp² hybridised carbon network having extended Π -conjugation and possesses a lot of potential to sink and channelize charge carriers through its 2D-circuit and enhances the photocatalytic activity of a semiconductor material. Besides this, graphene possesses a theoretical high surface area (2600 m²/g),^[9] extreme thermal conductivity (~ 3000 -5000 W m⁻¹ k⁻¹)^[10] and excellent carrier mobility ($\sim 10\ 000$ cm²V⁻¹s⁻¹) at room temperature,^[11] good optical transparency ($\sim 97.7\%$)^[11] and high Young's modulus (~ 1 TPa).^[12] Taking into account of its unique properties, several methods have already been developed for making graphene hybrid photocatalyst for numerous applications, like energy production and storage, water purification, organic pollutant degradation etc.^[13-26] In this regards, graphene based-materials like In₂S₃ nanosheets/graphene, TiO₂/RGO, ZnO/RGO, CdS/RGO and ZnO/graphene have been reported for the photocatalytic reduction of Cr(VI).

[27-31]

Iron oxyhydroxide (α -FeOOH) is richly available in water, soils, sediments, and rocks in the Earth's surface.^[32] Owing to its availability, nontoxic, resistance to corrosion and low cost, goethite (α -FeOOH) has been extensively used for water purification, organic pollutant degradation, human sensing application, rechargeable lithium-ion batteries, magnetic devices, electrode materials etc.^[33-39] Many researchers have fabricated various morphologies of α -FeOOH such as nanorods, urchin, nanospheres, array, pancake etc. and have evaluated their photocatalytic activity.^[40-43] Although, it possesses high absorptive power in the red light of visible region, the charge carrier recombination lowers its efficiency as a photocatalyst (1.9-2.2 eV).

Nanocomposites consisting of α -FeOOH and RGO have drawn considerable attention due to its wide application in various fields. Huang et al. have evaluated the photocatalytic activity of α -FeOOH/RGO towards the degradation of organic dyes.^[44] Yan et al. synthesised hexagonal-symmetry α -FeOOH crystals using RGO as a surfactant and tested its Li storage properties.^[45] The adsorption capacity of graphene/ α -FeOOH hydrogels towards removal of Cr(VI) and Pb (II) ions has been evaluated by Cong et al.^[46] Hu et al. has prepared α -FeOOH/RGO composite and implemented it as a supercapacitor.^[47] Peng et al. have evaluated the water purification properties of α -FeOOH/RGO composite.^[48] In this investigation, we have made a novel approach for the synthesis of well crystalline, phase pure and stable α -FeOOH nanorod/RGO composite without using any template or structural directing agent and studied the enhanced photocatalytic activity towards the reduction of Cr(VI) which is ascribed to the developed synergy between the 1D α -FeOOH nanorod over 2D graphene sheets. Previously, we have reported the facile hydrothermal route for the synthesis of graphene based semiconductor photocatalysts such as RGO/InGaZn mixed oxide,^[49] α -Fe₂O₃ nanorod/RGO composite^[50] and investigated their photocatalytic activity

towards hydrogen production and phenol degradation under visible light irradiation, respectively.

The priority of this work is to explore, (a) the role of RGO, (b) the effect of structural, optical and electronic property of α -FeOOH nanorod/RGO on the inhibition of electron-hole recombination in the photochemical process and (c) the developed synergism between α -FeOOH nanorod and RGO which enhances the photo catalytic activity towards the reduction of Cr(VI). Loading of 3wt% of RGO to α -FeOOH nanorod showed almost 4 times higher activity compared to the synthesised neat α -FeOOH nanorod. Several spectroscopic techniques have been used to derive the superior property of all synthesised α -FeOOH nanorod/RGO composite.

2. Experimental

2.1 Material

All the chemicals and reagents are of analytical grade and used without further purification. Iron nitrate ($\text{Fe}(\text{NO}_3)_3 \cdot 9\text{H}_2\text{O}$), Natural graphite powder, Potassium permanganent were procured from Sigma Aldrich Chemicals. Sulphuric acid (H_2SO_4), Hydrochloric acid (HCl), Sodium nitrate (NaNO_3) and Sodium hydroxide (NaOH) were obtained from Finar chemicals Limited.

2.2 Synthesis of graphene oxide (GO)

Graphene oxide was prepared by modified Hummer's method.^[51] Briefly, 1g of natural graphite powder with 1g of NaNO_3 was suspended in 46 mL of concentrated H_2SO_4 and the suspension was stirred for 30 mints by putting its container in an ice bath. Then, 8 g of KMnO_4 was slowly added to the suspension to obtain a purple-green colour solution which indicates the completion of the oxidation process. Now the container was transferred to a water bath to maintain the temperature of the solution around 40°C and stirred for 90 minutes. Then 100 mL of deionised water was added to the solution and stirred further for 30 minutes. After

that, 12 mL of 30% H₂O₂ solution was slowly added to the suspension and a golden-brown sol was obtained. The resultant solution was centrifuged and washed several times with deionised water to adjust its pH ~ 6. Finally, the obtained sample was dried at 80°C for 24 h.

2.3 Hydrothermal synthesis of α -FeOOH nanorods

Calculated amount of Fe(NO₃)₃ 9H₂O was dissolved in 20 mL of deionised water and its pH was adjusted to 12 by adding NaOH solution under vigorous stirring. Then, the obtained solution was sealed in a Teflon-line autoclave for hydrothermal treatment at 180 °C for 24 h. The obtained product was then subjected to centrifuge, washed with deionised water and finally dried at 80 °C for 24 h. The synthesised sample was designated as 0GFeOOH.

2.4 Hydrothermal synthesis of α -FeOOH nanorod/RGO

In a typical experiment, calculated amount of as synthesised GO was sonicated for 1 h in 40 mL deionised water to obtain a well separated mono-layers of GO. After that, the brown colour suspension of GO was added to the previously prepared Fe³⁺ precipitate and stirred for 30 minutes. Then, the rest of the procedure was kept same as the synthesis of α -FeOOH nanorods, described earlier. The loading amount of GO was varied like 1, 2, 3, and 4 wt % to α -FeOOH and are designated as 1GFOH, 2GFOH, 3GFOH and 4GFOH, respectively.

2.5 Analytical Characterisation

The Powder X-ray diffraction (PXRD) pattern of all the prepared photocatalysts were analyzed by Powder X-ray diffraction (PXRD) on Rigaku Miniflex (set at 30 kV and 15 mA) using CuK α radiation ($\lambda = 1.54 \text{ \AA}$) and recorded over the range $10^\circ < 2\theta < 60^\circ$ with a scan rate of 2°/min. UV-vis spectrophotometer (Varian Cary 100) was used to measure the optical absorbance of all the prepared photocatalysts in the region 200-800 nm with boric acid as the reference. VG Microtech Multilab ESCA 3000 spectrometer with a non-monochromatised Mg-K α X-ray source was used for the analysis of X-Ray photoelectron

spectroscopy (XPS). The C 1s peak of carbon at 284.9 eV was taken as reference for correction of the binding energy. Transmission electron microscopy (TEM) and high resolution transmission electron microscopy (HRTEM) images were taken on Philips TECNAI G² instrument at an accelerating voltage of 200 kV. Before TEM analysis, the powder particles was dispersed with ethanol and a very little amount was dripped on a carbon film coated on a 3 mm diameter fine-mesh copper grid and dried to make a film. Photoluminescence spectra of all the samples were recorded at room temperature using a LS 55 fluorescence spectrometer (PerkinElmer) with excitation at 300 nm. Current voltage of all the samples was measured using a pyrex electrochemical cell which was consisted of a prepared electrode as the working electrode. A Ag/AgCl electrode and a platinum wire were used as reference and counter electrode, respectively. A potentiostat was used to control the potential of the working electrode. An aqueous solution of Na₂SO₄ (0.1 M) was taken in the cell and its pH was maintained at 6. Under illumination conditions ($\lambda \geq 400$ nm), a potentiostat/galvanostat (Versastat 3, Princeton Applied Research) was used for the photoelectrochemical measurement. A 300 W Xe lamp was taken as visible light irradiation source. No photoresponse in the solution was shown by FTO.

2.6 Photocatalytic experiment

The photocatalytic performance of all synthesised catalysts was evaluated by the photoreduction of (Cr(VI)) under visible light radiation. The Cr(VI) solution (10mg/L) was prepared by dissolving K₂Cr₂O₇ in deionised water. The photocatalyst (1g/L) was dispersed in 50 mL of Cr(VI) solution and stirred for 30 min in dark condition to reach adsorption-desorption equilibrium. Then, the mixed suspension was exposed to visible light irradiation in an irradiation chamber (BS-02, Germany).

2.6.1 Measurement of Cr (VI) concentration

At certain time intervals, 2mL of mixed suspension was withdrawn and centrifuged to separate the photocatalyst. The colour of the obtained solution was developed using diphenylcarbazide (DPC) method introduced by Clesceri et al.^[52] and the concentration of Cr(VI) was determined by measuring its absorbance at 540 nm using a Cary-100 (Varian, Australia) spectrophotometer.

2.6.2 Experiment for oxygen evolution

The oxygen evolution test was carried out in batch reactor. About 50 mg of photocatalyst was suspended in 50 mL of 0.01(M) AgNO₃ solution. The solution was kept under stirring to avoid settling down of the particles at the bottom of reactor. Here, Ag⁺ act as sacrificial electron acceptor, suppress the recombination of electron with the hole and helps to oxidise H₂O to O₂. A 125 W medium pressure Hg visible lamp (≥ 400 nm) (Scientific Aids and Instruments Corporation (SAIC), Chennai) was used as the light source and 1 M NaNO₂ solution was used as the UV filter. To eliminate the dissolved gases from the reaction mixture, the suspension was purged with nitrogen before irradiation. The evolved gas was collected by water displacement method and analyzed off line by a GC-17A (Shimadzu) using a 5 A⁰ molecular sieve column in TCD mode. Digital Illuminance Meter (TES-1332A, Taiwan) with inbuilt Si-diode was used to measure the light intensity. The oxygen gas was confirmed after comparing the retention time of the only peak that appeared on the chromatogram with that of the standard.

3. Results and Discussions

3.1 Structural characterization

The powder X-ray diffraction (PXRD) patterns confirmed the structural characteristics and phase composition of pure α -FeOOH nanorods and α -FeOOH nanorods/RGO nanocomposites. Fig. 1 illustrates the XRD patterns of the as synthesized α -

FeOOH nanorods and α -FeOOH nanorods/RGO nanocomposites. The obtained XRD peaks are indexed to the orthorhombic α -FeOOH system corresponding to JCPDS File No. 81-0462. No impurity related peaks and well similar indexing planes are observed after loading of GO up to 4wt%. The crystal phase of all the synthesised photocatalysts is highly pure and the comparative broadening of all the reflection peaks shows the formation of the nanomaterial.

Moreover, the XRD analysis draw the following conclusions: (a) Introduction of RGO neither affects its phase purity nor its crystallinity which is more beneficial for its photocatalytic activity and (b) the disappearance of characteristics RGO peaks suggests its low amount of loading and well incorporation of α -FeOOH nanorods in between the Sp^2 hybridised-carbon monolayer of RGO sheets which leads to exfoliation and wrapping of RGO sheets during composite formation.^[31, 53] These above evidence are well supported by TEM analysis.

3.2 Raman analysis

To know the reduction GO to RGO as well as the composite formation between α -FeOOH nanorods and RGO, raman analysis has been carried out. Fig. 2 represents the raman spectra of GO and all the synthesised photocatalysts. The raman spectra of GO shows 'D' and 'G' band at 1350 and 1592 cm^{-1} respectively.^[54] Here, D band is assigned to the defects and disordering atomic arrangements of Sp^3 hybridised carbon atoms and the presence of G band is due to the plane vibration of Sp^2 hybridised carbon atoms of 2D layer of GO. In addition to that, its 2D band was found at 2661 and 2922 cm^{-1} which arises due to the second order raman scattering process.^[55] In case of α -FeOOH nanorod, the raman characteristics peaks are observed at 240, 296, 395, 476, 543 and 678 cm^{-1} (Fig. 2 (c)). All these fundamental raman vibration of α -FeOOH nanorod are due to the asymmetric stretching of metal and hydroxide group. The Raman spectra of all GO loaded α -FeOOH nanorod i.e, 1GFeOOH, 2GFeOOH,

3GFeOOH and 4GFeOOH gives the following evidences i.e, (1) their raman spectrum show both the D and G band of GO as well as all the fundamental raman vibrations of α -FeOOH nanorods which confirms about the composite formation during hydrothermal process. (2) In case composite, the shifting of both D and G band of GO (Fig. 2 (b)) strongly suggests about the strong interaction and well incorporation of metal oxy hydroxide cations on the negative surface of GO, and (3) The increase in the value of intensity ratio of D band and G band (I_D/I_G) of all nanocomposites compared GO (Table-1) confirms the reduction of oxygen functional groups on GO.^[56] All the RGO loaded α -FeOOH show higher I_D/I_G value than GO which strongly suggests the decrease of Sp^2 domain of GO.^[57] These above observations are consistent with our FESEM and TEM analysis.

3.3 Electron microscopy

The morphological characteristics and particle size of the synthesised photocatalysts were studied by FESEM and TEM analysis. Fig. 3 displays the FESEM analysis of α -FeOOH and 3GFeOOH composite. A rod like morphology with nanometre-sized α -FeOOH is clearly observed from Fig. 3 (a). The obtained α -FeOOH nanorods possess a uniform shape and well dispersed structure. Fig. 3(b) presents micrometer-sized structure of α -FeOOH nanorod/RGO composite (3GFeOOH) where α -FeOOH nanorods are embedded and uniformly distributed on the flat surface of RGO sheets. The high resolution magnified analysis of 3GFeOOH shows that there is a well decoration of α -FeOOH nanorods on RGO sheets. The energy dispersive X-ray (EDX) spectroscopy measurements of 3GFeOOH show the presence of C, O and Fe (Fig. 3(d)). In case of composite, the folding and stacking of RGO sheets is avoided due to the well allocation of α -FeOOH nanorods which increases the stability of individual graphene sheets. This also gives a good platform for better transportation of photoexcited electron to graphene sheets which plays a major role in enhancing the photocatalytic activity of α -FeOOH nanorods. Fig. 4(a) and (b) & (c)

represents the TEM images of α -FeOOH and 3GFeOOH. From the TEM micrograph of α -FeOOH, it is observed that α -FeOOH consisted of nanorod morphology which are elongated longitudinally to a finite dimension with average length 600-650 nm and width 50-55 nm. From the images of 3GFeOOH, the well dispersion of the α -FeOOH nanorods over RGO surface is clearly observed. It was found that the oxygenated groups on the GO surface provide a good platform for well anchoring of α -FeOOH nanorods on its 2D-surface which avoids the restacking of graphene sheets, and hence increases the stability of individual graphene sheets.^[58] This stability of RGO plays a crucial role in the photocatalytic performance of 3GFOOH. The average length and width of the α -FeOOH nonorods in 3GFeOOH was found to be 450-500 nm and 30-35 nm, respectively. This change in the aspect ratio of α -FeOOH nanorods may be due to crystal growth inhibition effect of α -FeOOH nanorods in presence of reduced graphene oxide.^[49] Hence, the small size of α -FeOOH nanorods played a crucial role in enhancing the photocatalytic activity because small particle size favours the photogenerated electrons to reach the surface easily for better utilisation in the photochemical process.^[59] The facile transport of electrons by the reduced graphene sheets played a vital role in enhancing the photocatalytic activity of the nanocomposite. Fig. 4(e) illustrates the selected area electron diffraction (SAED) pattern of 3GFeOOH. Several bright continuous concentric rings are observed from the SAED pattern due to the diffraction from the (110), (130), (111), and (210) planes of α -FeOOH nonorods which indicates the polycrystalline nature of the prepared α -FeOOH nanorods. It is also consistent well with the XRD data. Moreover, its crystallinity character is confirmed from the obtained lattice fringes of 3GFeOOH, presented in Fig. 4(d)). The obtained lattice fringe spacing of 0.269 nm ensures that the 130 plane of α -FeOOH and is well agreed with the XRD analysis.

3.4 DRUV-vis spectra

In order to know the optical absorption characteristics of all the photocatalysts, DRUV-vis spectra has been recorded. Fig. 5(a) illustrates the optical absorption spectra of all the photocatalysts. From the absorption spectra, it can be clearly observed that all the photocatalysts show absorption band in the visible region which is due to $2(^6A_1) \rightarrow ({}^4T_1)$ ligand field transition of Fe^{3+} ,^[60] while all the RGO loaded photocatalysts showed slight larger absorption edge which is due to the black body property of RGO.^[61] This above observation suggests that, during photoelectrochemical process RGO modifies the fundamental process of electro-hole pair formation of α -FeOOH nanorod.^[61]

The band gap energy of all synthesised α -FeOOH and α -FeOOH/RGO composites was calculated by using following equation^[62]

$$ah\nu = A(h\nu - E_g)^n$$

Where a , n , A , and E_g are the absorption coefficient, light frequency, proportionality constant, and band gap energy, respectively and n describes the type of the transition in a semiconductor *i.e.* $n = 1/2$ for direct transition and $n = 2$ for indirect transition. The value of n for all the prepared samples was taken as $1/2$ which confirms the optical transition of α -FeOOH and α -FeOOH /RGO composites are directly allowed.^[50] The band gap of all the synthesized photocatalysts are shown in Fig. 5(b). The band gap energy of all the photocatalysts is estimated from the plot of $(ah\nu)^n$ vs. $h\nu$ by extrapolating the straight line to the X axis intercept. The band gap energy of 0GFeOOH, 1GFeOOH, 2GFeOOH, 3GFeOOH and 4GFeOOH were found to be 2.004, 1.99, 1.98, 1.945 and 1.925 eV, respectively. This above band gap energy estimation of all prepared α -FeOOH/RGO composites confirms that the introduction of RGO doesn't not strongly effect on the optical absorption property of α -FeOOH while its presence shifts the absorption edge of all samples towards red region.^[50]

3.5 Photoluminescence spectra

The PL study of all the photocatalysts has been carried out to know the migration, transfer and recombination process of electron-hole pair.^[63,64] The PL spectra of all the photocatalysts has been recorded at room temperature with an excitation of 300 nm which is represented in Fig. 6. From the PL spectra, it is observed that α -FeOOH shows more intense peak compared to others. As PL intensity is direct measurement of electron-hole recombination, the more intense peak of α -FeOOH indicates its high rate of electron-hole recombination. Since photocatalytic activity of semiconductor is directly dependant on the concentration of photogenerated charge carries,^[64, 65] that's why α -FeOOH showed lower photocatalytic activity. But all the RGO loaded α -FeOOH showed less intense PL compared to neat α -FeOOH. Among which 3GFeOOH showed lowest PL intensity. This low PL intensity suggests that more number of excited electrons are trapped and stably transferred through the interface.^[66] Hence, in case of 3GFeOOH, there is a minimal recombination of charge carrier which proves its better photocatalytic activity.

3.6 Time resolved photoluminescence spectra

For the better understanding of the photoexcited electron (e^-) transfer dynamics from the conduction band of α -FeOOH to graphene sheets, time-resolved photoluminescence measurement has been carried out to calculate decay components. The time -resolved photoluminescence spectra for 0GFeOOH and 3GFeOOH is shown Fig. 7. Table-2 represents the well fitted decay dynamics for 0GFeOOH and 3GFeOOH. This shows a longer decay time value for 3GFeOOH than that of neat FeOOH which is due to the effective charge transfer across the interface of graphene and α -FeOOH.^[67] In addition to that the decrease of fractional contribution (f_1 , f_2 and f_3) and increase of decay time (τ_1 , τ_2 and τ_3) also suggests a decrease in density of trapped states. This may achieved by the strong attachment of 1D α -FeOOH nanorods over 2D graphene sheets which leads to facilitate the photoexcited e^- of α -FeOOH to graphene sheets.^[67] As the relaxation or decay strongly depends of densities of

initial and final states, the longer average decay time ($\langle\tau^2\rangle$) of 3GFeOOH than neat α -FeOOH clearly suggests that good charge separation occurs after introduction graphene to α -FeOOH which displays a key role for its enhanced photocatalytic activity.

3.7 Photoelectrochemical performance

In order to correlate the photoelectrochemical properties with the photocatalytic activity of the synthesised photocatalysts, the photocurrent measurement of α -FeOOH (0GFeOOH) and 3GFeOOH composite was carried out. Fig. 8(a) and 8(b) represents the photocurrent of 0GFeOOH and 3GFeOOH in dark and visible light illumination, respectively. It was found that appreciably no photocurrent was generated under dark condition from both of the prepared electrodes while a photocurrent generation in anodic direction was observed under irradiation of light ($\lambda \geq 400$ nm). The photocurrent of both the photocatalysts was increased with positive applied bias which shows their n-type semiconducting property.^[64] The photocurrent density of 0GFeOOH and 3GFeOOH was found to be 0.63 and 1.81 mA/cm², respectively. It is well known that the photocurrent density of an n-type semiconductor depends upon the concentration of electrons. That means, 3 times higher photocurrent density of 3GFeOOH than that of neat α -FeOOH indicates that more number of free electrons are transported in the circuit in case of 3GFeOOH photoelectrode.^[68-71] Hence, there is a good separation of charge carriers in case of 3GFeOOH which can be ascribed to the strong interaction of α -FeOOH with the flat 2D RGO sheets. The excellent photoelectrochemical property of 3GFeOOH is in well agreement with PL study.

3.8 Photocatalytic activity

The photocatalytic reduction of Cr(VI) over 0GFeOOH, 1GFeOOH, 2GFeOOH 3GFeOOH and 4GFeOOH was performed under visible light irradiation. The percentage of

Cr(VI) reduction was monitored at different time intervals such as 30, 60, 90, 120, 150, 180 and 210 minutes taking Cr(VI), 10 mg/L and 3GFeOOH photocatalysts (1g/L) (Fig. 9). It was found that after 180 minutes, no effective reduction of Cr(VI) was observed. So, the reduction of Cr(VI) by all photocatalysts was performed at 3h.

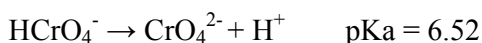
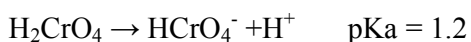
Fig. 10 illustrates the normalised temporal concentration of changes (C/C_0) of Cr(VI) during the photocatalytic process. It was observed that all the RGO promoted α -FeOOH nanorod showed better photocatalytic activity compared neat α -FeOOH nanorod. The photocatalytic activity of α -FeOOH nanorod gradually increased up to 3wt% loading of RGO and started decreasing on 4 wt% loading of RGO (Fig. 10). 3GFeOOH (1g/L) showed highest i.e. 94% reduction of Cr(VI) (10 mg/L), whereas α -FeOOH nanorod showed only 26%. That means at pH = 2, 3wt% loading RGO to α -FeOOH nanorod showed almost 4 times greater activity towards the reduction of Cr(VI) under visible light irradiation.

Since pH strongly affects the photoreduction of Cr(VI), the effect of pH was studied in the range 2-10 by taking 3GFeOOH (1g/L) photocatalyst. It was observed that with increasing pH, the photocatalytic activity of the composite decreases (Fig. 11). At low pH, Cr species exists as HCrO_4^- and as the pH increases it changes to $\text{Cr}_2\text{O}_7^{2-}$. That means at low pH, the surface of the photocatalysts gets highly protonated and becomes more positive for better accumulation of HCrO_4^- ions. At higher pH value, the surface of photocatalyst becomes negative which tends to repel the $\text{Cr}_2\text{O}_7^{2-}$ ions and hence decreases its photocatalytic activity. The photocatalytic activity exhibits a following order: 0GFeOOH < 1GFeOOH < 2GFeOOH < 4GFeOOH < 3GFeOOH. A comparison of photoreduction capacity of α -FeOOH/RGO composite with other reported graphene based photocatalysts is shown in table-3. The direct comparison of α -FeOOH/RGO composite with other photocatalysts is difficult due to the different experimental conditions. But, the photoreduction efficiency of 3GFeOOH towards the reduction of Cr(VI) is quite impressive.

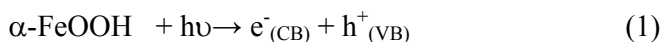
4 Mechanism of photocatalytic reduction of Cr (VI)

4.1 Mechanism of photocatalytic reduction of Cr (VI) over α -FeOOH nanorod

Generally, H_2CrO_4 and HCrO_4^- are the predominant form of Cr(VI) at low concentration while at high concentration solution Cr(VI) exists in $\text{Cr}_2\text{O}_7^{2-}$ form. However, pH plays a major role for their inter conversion.^[72] At acidic medium, the HCrO_4^- is the predominant form while CrO_4^{2-} is found at neutral or basic solution of Cr(VI). The equilibrium of Cr (VI) in solution is^[73]

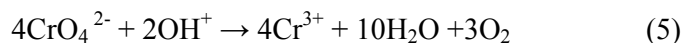


Earlier, it has been reported in most of the cases that the photoreduction of Cr(VI) is easier in acidic condition compared neutral or basic medium.^[74-76] In this respect, the effect of pH on the photoreduction of Cr(VI) has been studied. When α -FeOOH nanorod photocatalyst is exposed to visible light irradiation, the excitation of electron occurs from its valence band to conduction band. This leads to generation of photoexcited electrons at its conduction band and holes in its valence band. At the conduction band of α -FeOOH nanorod, the photoexcited electrons (e^-) are utilised for the reduction of Cr(VI) to Cr(III), while at the same time the holes (h^+) oxidise water molecule to O_2 in its valence band. The photocatalytic performance of α -FeOOH nanorod is restricted due to its flash recombination of $e^-_{(\text{CB})}$ and $h^+_{(\text{VB})}$. As the photoreduction of Cr(VI) has been carried out in its low concentration, there is great possibility of the presence of Cr as CrO_4^{2-} form. At pH=2, the photoreduction of Cr(VI) over α -FeOOH nanorod can be described by the following equations,





The net reaction is as follows



4.1.1 Test for Oxygen Evolution

In order to give the evidence for O₂ evolution in the valence band of photocatalyst, the photocatalytic oxygen evolution was carried out by suspending the synthesized photocatalysts in aq. AgNO₃ solution. It was observed that all the synthesized samples could able to produce oxygen which is presented in Fig.12. Among all, 3GFeOOH could able to evolve highest amount oxygen i.e., 181 μmol/h whereas 0GFeOOH, 1GFeOOH, 2GFeOOH and 4GFeOOH gave 86 μmol/h, 112 μmol/h, 143 μmol/h, 159 μmol/h respectively. It is observed that the rate of oxygen evolution followed the same order to that of Cr(VI) reduction activity under visible light. This observation gives well support to our proposed mechanism for Cr(VI) reduction under visible light irradiation.

4.2 Mechanism of photocatalytic reduction of Cr(VI) over α-FeOOH nanorod/RGO composite

In the photochemical process, graphene sheets act as potential sinker which traps the photoexcited electrons from the conduction band of α-FeOOH and channelizes through its extended Π-conjugation carbon network. This channelization of photoexcited electron of α-FeOOH is easily available on the graphene surface for the Cr(VI) reduction to Cr(III). Thus, there is a great possibility of Cr(VI) reduction to Cr(III) on the great graphene sheets. Scheme-1 gives an account of this possible mechanism of photoreduction of Cr(VI) to Cr(III) over 3GFeOOH under visible light irradiation.

This can be confirmed from the XPS spectra of α -FeOOH/RGO composite, obtained after the reaction. The core level XPS spectra (i) and (ii) in Fig. 13(a) illustrate the constituent elements in 3GFeOOH before and after photoreduction of Cr(VI). The detailed XPS analysis in the region of C1s, Fe2p, O1s and Cr 2p in 3GFeOOH is shown in Fig. 13. The high resolution spectrum of C 1s (Fig. 13(b)) shows two peaks at binding energy values of 284.7 and 289.4 eV. Among which the peak corresponds to the binding energy 284.7 eV is assigned to sp^2 aromatic C-C bond of RGO and the peak at higher binding energy value of 289.4 eV corresponds to oxygenated carbon species of RGO. [66, 77] The core level XPS spectra of C 1s in GO is shown as the supplementary information (Figure S1†). The core level XPS spectrum of C 1s shows two peaks corresponds to its binding energy 284.9 and 289.1 assigned to the sp^2 aromatic C-C bond and oxygenated carbon species of GO, respectively. [78] The relative intensity associated with oxygenated carbon species in 3GFeOOH is appreciably less as compared to GO which confirm the significant reduction GO to RGO during hydrothermal process. [49, 50] The XPS spectra of O 1s (Fig. 13(c)) shows a peak at binding energy value of 529.8 eV which is attributed to the lattice oxygen of α -FeOOH. [79] The XPS spectra of Fe 2p (Fig. 13(d)) shows two peaks centred at 711.4 eV and 724.6 eV, assigned to Fe 2p_{3/2} and Fe 2p_{1/2}, respectively which is in well agreement with the previously reported binding energy value for Fe³⁺ in α -FeOOH. [80] The wide scan spectra of 3GFeOOH after photoreduction of Cr(VI) shows two new peaks around 575-595 eV along with the peaks for carbon, iron and oxygen. The XPS scan of Cr 2p region is shown in Fig. 12(e). The photo electron peaks at 577.7 and 588.5 eV correspond to the binding energies of Cr 2p_{3/2} and Cr 2p_{1/2} for both Cr(III) and Cr(VI), [80] respectively which may due to the accumulation of Cr(III) on graphene surface after the photoreduction of Cr(VI). This evidence supports the possible mechanism of deposition of Cr(III) on the graphene surface as the electrons are flowing from the conduction of α -FeOOH nanorod to graphene.

5. Role of RGO

The enhanced photocatalytic activity of α -FeOOH nanorod/RGO composite strongly depends on its fabrication and loading amount of RGO. The advantages of RGO loading can be ascribed to the following points: (1) Effect of α -FeOOH nanorod complexation with RGO, (2) Increase of light harvesting capacity of α -FeOOH nanorod and (3) Fast transfer of photo excited electron to RGO sheets and efficient separation of photogenerated electron-hole pairs.

Briefly, it was observed from XRD analysis that the phase purity as well as the crystallinity of α -FeOOH nanorod is well maintained up to 4wt% RGO loading. Electron microscopic analysis clearly suggests lowering of agglomeration of α -FeOOH nanorod and stacking of RGO sheets which plays a crucial role in the photocatalytic activity of α -FeOOH nanorod/RGO. It has already been discussed in TEM part that the length and width of α -FeOOH nanorod is decreased, may be due to growth inhibition effect of α -FeOOH in presence of RGO. The small size of α -FeOOH may favour the transfer of electron from bulk to its surface which plays an important role in its photocatalytic activity. In addition, the strong attachment of α -FeOOH on the graphene sheets gives more beneficial effect for better migration of photoexcited electron from the conduction band of α -FeOOH to graphene sheets. Thus, the flash recombination of electron-hole is minimised and beneficial for the enhancement of photocatalytic activity of α -FeOOH nanorod towards the reduction of Cr(VI) to Cr(III) under visible light irradiation.

The optical absorption property of α -FeOOH nanorod and α -FeOOH nanorod/RGO composite has already been discussed in DRUV-vis spectra analysis section. It can be clearly observed that the light absorption capacity of α -FeOOH nanorod increased in the visible region after RGO complexation. This is due to the black body property of RGO. This is quite

similar to the previously reported materials like TiO₂/RGO [21] and ZnO/Graphene [24] composites. Hence, the increase in light harvesting capacity of α -FeOOH certainly helps to produce more no photoexcited electrons on its conduction band which strongly affect its photoreduction efficiency towards Cr(VI) reduction under visible light irradiation.

In PL study section, it has been already discussed about the migration, transfer and recombination process of electron-hole for all synthesised photocatalysts. Among all the synthesised photocatalysts, 3GFeOOH showed lowest peak intensity. This observation clearly suggests about the better separation of electron-hole and suppression of recombination, achieved due to the presence of graphene sheets. In addition to that, the photocurrent density of 3GFeOOH was found to be 1.81 mA/cm² which almost 3 times greater than neat α -FeOOH nanorod. This result suggests that more no of electrons are flowing through the circuit in case of graphene hybrid material. That means, in case composite material more no electrons are available for photochemical reaction. In the photochemical process, graphene sheets acts as potential sinker which traps the photoexcited electron from the conduction band of α -FeOOH and channelizes through its extended Π -conjugation carbon network. This channelization of photoexcited electron of α -FeOOH is easily available on the graphene surface for the Cr(VI) reduction to Cr(III). Thus, there is a great possibility of Cr(VI) reduction to Cr(III) on the graphene sheets.

6. Conclusions

In summary, the highly active α -FeOOH nanorod/RGO composites were successfully prepared by a facile hydrothermal route without using any template. The photoexcited electrons of α -FeOOH nanorods can be easily trapped by the graphene sheets and transported through the extended Π -conjugated carbon network to the substrate molecules. This leads to suppress charge recombination, improve interfacial charge transfer

processes, providing much more active adsorption sites and photocatalytic reaction centres, which significantly enhances the photocatalytic activity of all the nanocomposites. The amount of RGO loading played a crucial role in the photocatalytic activity, among which 3wt% loading of RGO to α -FeOOH showed highest photoreduction of Cr(VI) i.e. 94% under visible light irradiation. The highest photocatalytic activity of 3GFeOOH is well explained in terms of its lowest PL intensity, high photocurrent density (1.81 mA/cm^2) and its time-resolved photoluminescence spectra measurements which shows longer average time decay value ($\langle\tau\rangle$) ie 4.13 ns than neat α -FeOOH. Hence, it can be concluded that the developed α -FeOOH nanorod/RGO composite may be a promising candidate for solar cell as well as fuel cell applications.

Acknowledgements

The authors are very much thankful to Prof. B.K. Mishra, Director, CSIR-IMMT for giving permission to publish the work. The authors are also thankful to Dr. Y. S. Chaudhary and K. K. Nanda for the TRPL analysis. The financial assistance from BRNS in form of project (GAP-215) is greatly acknowledged.

REFERENCES

- [1] K. Zhigang, H. Qing, Z. Hong and Y. Zengliang, *Environ. Sci. Technol.*, 2011, **45**, 7841–7847.
- [2] D. E. Kimbrough, Y. Cohen, A. M. Winer, L. Crelman and C. Mabuni, *Environ. Sci. Technol.*, 1999, **29**, 1-46.
- [3] N. M. Dogan, C. Kantar, S. Gulcan, C. J. Dodge, B. C. Yilmaz and M. A. Mazmanci, *Environ. Sci. Technol.*, 2011, **45**, 2278–2285.
- [4] H. Ma, Y. Zhang, Q. Hu, D. Yan, Z. Yu and M. Zhai, *J. Mater. Chem.*, 2012, **22**, 5914–5916.

- [5] J. Wang, X. Li, X. Li, J. Zhu and H. Li, *Nanoscale*, 2013, **5**, 1876.
- [6] Y. Qu, W. Zhou, L. Jiang and H. Fu, *RSC Adv.*, 2013, **3**, 18305–18310.
- [7] G. Dong and L. Zhang, *J. Phys. Chem. C*, 2013, **117**, 4062–4068.
- [8] N. S. Waldmann and Y. Paz, *J. Phys. Chem. C*, 2010, **114**, 18946–18952.
- [9] B. Cheng, J. M. Russell, W. Shi, L. Zhang and E. T. Samulski, *J. Am. Chem. Soc.*, 2004 **126**, 5972-5973.
- [10] Y. Wu, Y. Cui, L. Huynh, C. Barlett and C. M. Lieber, *Nano Lett.*, 2004, **4**, 433-436.
- [11] Z. W. Pan, Z. R. Dai and Z. L. Wang, *Science*, 2001, **291**, 1947-1949.
- [12] S. Iijima, *Nature*, 1991, **354**, 56-58.
- [13] Y. T. Liang, B. K. Vijayan, K. A. Gray and M. C. Hersam, *Nano Lett.*, 2011, **11**, 2865–2870.
- [14] J. Zhou, G. Tian, Y. Chen, X. Meng, Y. Shi, X. Cao, K. Pana and H. Fu, *Chem. Commun.*, 2013, **49**, 2237-2239.
- [15] H. M. Sun, L. Y. Cao and L. H. Lu, *Nano Res.*, 2011, **4**, 550–562.
- [16] N. W. Li, M. B. Zheng, X. F. Chang, G. B. Ji, H. L. Lu, L. P. Xue, L. J. Pan and J. M. Cao, *J. Solid State Chem.*, 2011, **184**, 953–958.
- [17] X. Y. Zhang, H. P. Li, X. L. Cui and Y. H. Lin, *J. Mater. Chem.*, 2010, **20**, 2801–2806.
- [18] W. Q. Fan, Q. H. Lai, Q. H. Zhang and Y. Wang, *J. Phys. Chem. C*, 2011, **115**, 10694–10701.
- [19] L. S. Zhang, L. Y. Jiang, H. J. Yan, W. D. Wang, W. Wang, W. G. Song, Y. G. Guo and L. J. Wan, *J. Mater. Chem.*, 2010, **20**, 5462–5467.
- [20] M. Q. Yang and Y. J. Xu, *Phys. Chem. Chem. Phys.*, 2013, **15**, 19102-19118.
- [21] Y. Zhang, Z. R. Tang, X. Fu and Y. J. Xu, *ACS Nano*, 2011, **5**, 7426-7435.
- [22] Y. Zhang, Z. R. Tang, X. Fu and Y. J. Xu, *ACS Nano*, 2010, **4**, 7303-7314.
- [23] Y. Zhang, N. Zhang, Z. R. Tang and Y. J. Xu, *ACS Nano*, 2012, **6**, 9777-9789.

- [24] N. Zhang, M. Q. Yang, Z. R. Tang and Y. J. Xu, *ACS Nano*, 2014, **8**, 623-633.
- [25] N. Zhang, Y. Zhang, X. Pan, M. Q. Yang and Y. J. Xu, *J. Phys. Chem. C.*, 2012, **116**, 18023-18031.
- [26] N. Zhang, Y. Zhang, X. Pan, X. Fu, S. Liu and Y. J. Xu, *J. Phys. Chem. C.*, 2011, **115**, 23501-23511
- [27] X. An, J. C. Yu, F. Wang, C. Li and Y. Li, *Appl. Catal., B*, 2013, **129**, 80– 88.
- [28] X. Liu, L. Pan, T. Lv, G. Zhu, T. Lu, Z. Sun and C. Sun, *RSC Adv.*, 2011, **1**, 1245–1249.
- [29] X. Liu, L. Pan, Q. Zhaob, T. Lv, G. Zhu, T. Chen, T. Lu, Z. Sun and C. Sun, *Chem. Eng. J.*, 2012, **183**, 238– 243.
- [30] X. Liu, L. Pan, T. Lv, T. Lu, G. Zhu, Z. Sun and C. Sun, *Chem. Commun.*, 2011, **47**, 11984–11986.
- [31] X. Liu, L. Pan, T. Lv, T. Lu, G. Zhu, Z. Sun and C. Sun, *Catal. Sci. Technol.*, 2011, **1**, 1189–1193.
- [32] L. Deguillaume, M. Leriche, K. Desboeufs, G. Mailhot, C. George and N. Chaumerliac, *Chem. Rev.*, 2005, **105**, 3388.
- [33] G. Zhang, S. Wang and F. Yang, *J. Phys. Chem. C*, 2012, **116**, 3623–3634.
- [34] H. Li, W. Li, Y. Zhang, T. Wang, B. Wang, W. Xu, L. Jiang, W. Song, C. Shu and C. Wang, *J. Mater. Chem.*, 2011, **21**, 7878–7881.
- [35] P. V. Adhyapak, U. P. Mulik, D. P. Amalnerkar and I. S. Mull, *J. Am. Ceram. Soc.*, 2013, **96**, 731–735.
- [36] S. Krehula, S. Popovi and S. Musi, *Mater. Lett.*, 2002, **54**, 108–113.
- [37] J. F. Boily, N. Nilsson, P. Persson and S. Sjoberg, *Langmuir*, 2000, **16**, 5719–5729.
- [38] M. Charles and J. R. Flynn, *Chem. Rev.*, 1984, **84**, 31–41.
- [39] D. E. Zhang, X. J. Zhang, X. M. Nia and H. G. Zheng, *Mater. Lett.*, 2006, **60**, 1915–1917.

- [40] X. Zhou, H. Yang, C. Wang, X. Mao, Y. Wang, Y. Yang and G. Liu, *J. Phys. Chem. C.*, 2010, **114**, 17051–17061.
- [41] M. Hojamberdiev, G. Zhu, A. Eminov and K. Okada, *J. Clust. Sci.*, 2013, **24**, 97–106.
- [42] L. Songa and S. Zhangb, *Eng. Aspects.*, 2009, **348**, 217–220.
- [43] S. Kakuta, T. Numata and T. Okayama, *Catal. Sci. Technol.*, 2014, **4**, 164–169.
- [44] G. Huang, C. Zhang, Y. Long, J. Wynn, Y. Liu, W. Wang and J. Gao1, *Nanotechnology*, 2013, **24**, 395601.
- [45] C. Zhang, J. Zhu, X. Rui, J. Chen, D. Sim, W. Shi, H. H. Hng, T. M. Lim and Q. Yan, *CrystEngComm.*, 2012, **14**, 147–153.
- [46] H. P. Cong, X. C. Ren, P. Wang and S. H. Yu, *ACS Nano*, 2012, **6**, 2693–2703.
- [47] H. Xu, Z. Hu, A. Lu, Y. Hu, L. Li, Y. Yang, Z. Zhang and H. Wu, *Materials Chemistry and Physics*, 2013, **141**, 310–317.
- [48] F. Peng, T. Luo, L. Qiu and Y. Yuan, *Mater. Res. Bull.*, 2013, **48**, 2180–2185.
- [49] S. Martha, D. K. Padhi and K. M. Parida, *ChemsusChem*, 2014, **7**, 585–597.
- [50] G. K. Pradhan, D. K. Padhi and K. M. Parida, *ACS Appl. Mater. Interf.*, 2013, **5**, 101–9110.
- [51] W. S. Hummers and R. E. Offeman, *J. Am. Chem. Soc.*, 1958, **80**, 1339–1339.
- [52] L. S. Clesceri, A. E. Greenberg and A. D. Eaton, *American Public Health Association: Washington*, 1998, 366–368,
- [53] Y. L. Chen, Z. A. Hu, Y. Q. Chang, H. W Wang, Z. Y. Zhang, Y. Y. Yang and H. Y. Wu, *J. Phys. Chem. C* 2011, **115**, 2563–2571.
- [54] K. A. Mkhoyan, A. W. Contryman, J. Silcox, D. A. Stewart, G. Eda, C. Mattevi, S. Miller and M. Chhowalla, *Nano Lett.*, 2009, **9**, 1058.
- [55] F. Tuinstra and J. L. Koenig, *J. Chem. Phys.*, 1970, **53**, 1126.

- [56] J. Qiu, P. Zhang, M. Ling, S. Li, P. Liu, H. Zhao and S. Zhang, *ACS Appl. Mater. Interf.*, 2012, **4**, 3636–3642.
- [57] M. S. A. S. Shah, A. R. Park, K. Zhang, J. H. Park and P. J. Yoo, *ACS Appl. Mater. Interf.*, 2012, **4**, 3893–3901.
- [58] H. Seema, K. C. Kemp, V. Chandra and K. S Kim, *Nanotechnology*, 2012, **23**, 355705.
- [59] K. M. Parida, K. H. Reddy, S. Martha, D. P. Das and N. Biswal, *Int. J. Hydrogen Energy*, 2010, **35**, 12161-12168.
- [60] R. M. Cornell and U. Schwertmann, *The Iron Oxide Book, 2nd ed.; Wiley-VCH: Weinheim, Germany*, 2003, 147.
- [61] L. W. Zhang, H. B. Fu and Y. F. Zhu, *Adv. Funct. Mater.*, 2008, **18**, 2180–2189.
- [62] K. M. Parida, A. Nashim and S. K. Mahanta, *Dalton Trans.*, 2011, **40**, 12839-12845.
- [63] K. M. Parida, S. Martha, D. P. Das and N. Biswal, *J. Mater. Chem.*, 2010, **20**, 7144–714.
- [64] S. Martha, K. H. Reddy, N. Biswal and K. M. Parida, *Dalton Trans.*, 2012, **41**, 14107-14116.
- [65] A. Mukherji, B. Seger, G. Q. Lu and L. Wang, *ACS Nano*, 2011, **5**, 3483–3492.
- [66] M. S. A. S. Shah, K. Zhang, A. R. Park, K. S. Kim, N. G. Park, J. H. Parkab and P. J. Yoo, *Nanoscale*, 2013, **5**, 5093-5101.
- [67] K. K. Nanda, S. Swain, B. Satpati, L. Besra and Y. S. Chaudhary, *RSC Adv.*, 2013 (accepted), DOI: 10.1039/C3RA47024E.
- [68] X. Y. Zhang, H. P. Li, X. L. Cui and Y. Lin, *J. Mater. Chem.*, 2010, **20**, 2801-2806.
- [69] N. Zhang, Y. Zhang and Y. J. Xu, *Nanoscale*, 2012, **4**, 5792–5813.
- [70] F. Schedin, A. K. Geim, S. V. Morozov, E. M. Hill, P. Blake, M. I. Katsnelson and K. S. Novoselov, *Nat. Mater.*, 2007, **6**, 652–655.
- [71] S. Watcharotone, D. A. Dikin, S. Stankovich, R. Piner, I. Jung, G. H. B. Momett, G. Evmenenko, S. E. Wu, S. F. Chen and C. P. Liu, *Nano Lett.*, 2007, **7**, 1888–1892

- [72] C. M. Welch, O. Nekrassova and R. G. Compton, *Talanta*, 2005, **65**, 74–80.
- [73] Z. Ke, Q. Huang, H. Zhang and Z. Yu, *Environ. Sci. Technol.*, 2011, **45**, 7841–7847.
- [74] L. Wang and X. Z. Jiang, *Environ. Sci. Technol.*, 2008, **42**, 8492–8497.
- [75] T. Cserfalvi, P. Mezie, *J. Anal. At. Spectrom.*, 1994, **9**, 345–349.
- [76] D. P. Das, K. Parida, B. R. De, *J. Mol. Catal. A: Chem.*, 2006, **245**, 217–224.
- [77] M. S. A. S. Shah, A. R. Park, K. Zhang, J. H. Park and P. J. Yoo, *ACS Appl. Mater. Interf.*, 2012, **4**, 2107–2115.
- [78] G. C. Behera, K. M. Parida and P.K. Satapathy, *RSC adv.*, 2013, **3**, 4863-4866.
- [79] T. Yamashita and P. Hayes, *Appl. Surf. Sci.* 2008, **254**, 2441–2449.
- [80] H. Jabeen, V. Chandra, S. Jung, J. W. Lee, K. S. Kim and S. B. Kim, *Nanoscale*, 2011, **3**, 3583.